

Article

Impact of COVID-19 Induced Lockdown on Environmental Quality in Four Indian Megacities Using Landsat 8 OLI and TIRS-Derived Data and Mamdani Fuzzy Logic Modelling Approach

Sasanka Ghosh ¹, Arijit Das ², Tusar Kanti Hembram ², Sunil Saha ²,
Biswajeet Pradhan ^{3,*} and Abdullah M. Alamri ⁴

¹ Department of Geography, Kazi Nazrul University, Asansol 713340, West Bengal, India; sasankaghoshsg@gmail.com

² Department of Geography, University of Gour Banga, Malda 732103, West Bengal, India; Arijit3333@gmail.com (A.D.); tusarpurulia1991@gmail.com (T.K.H.); sunilgeo.88@gmail.com (S.S.)

³ Centre for Advanced Modeling and Geospatial Information Systems (GIS), Faculty of Engineering and Information Technology, University of Technology Sydney, Sydney, NSW 2007, Australia

⁴ Department of Geology & Geophysics, College of Science, King Saud University, P.O. Box 2455, Riyadh 11451, Saudi Arabia; amsamri@ksu.edu.sa

* Correspondence: Biswajeet.Pradhan@uts.edu.au

Received: 10 June 2020; Accepted: 3 July 2020; Published: 7 July 2020



Abstract: The deadly COVID-19 virus has caused a global pandemic health emergency. This COVID-19 has spread its arms to 200 countries globally and the megacities of the world were particularly affected with a large number of infections and deaths, which is still increasing day by day. On the other hand, the outbreak of COVID-19 has greatly impacted the global environment to regain its health. This study takes four megacities (Mumbai, Delhi, Kolkata, and Chennai) of India for a comprehensive assessment of the dynamicity of environmental quality resulting from the COVID-19 induced lockdown situation. An environmental quality index was formulated using remotely sensed biophysical parameters like Particulate Matters PM₁₀ concentration, Land Surface Temperature (LST), Normalized Different Moisture Index (NDMI), Normalized Difference Vegetation Index (NDVI), and Normalized Difference Water Index (NDWI). Fuzzy-AHP, which is a Multi-Criteria Decision-Making process, has been utilized to derive the weight of the indicators and aggregation. The results showing that COVID-19 induced lockdown in the form of restrictions on human and vehicular movements and decreasing economic activities has improved the overall quality of the environment in the selected Indian cities for a short time span. Overall, the results indicate that lockdown is not only capable of controlling COVID-19 spread, but also helpful in minimizing environmental degradation. The findings of this study can be utilized for assessing and analyzing the impacts of COVID-19 induced lockdown situation on the overall environmental quality of other megacities of the world.

Keywords: COVID-19 pandemic; spatiotemporal analysis; environmental quality; PM₁₀ concentration; GIS; remote sensing

1. Introduction

Environmental deterioration has emerged as a rising alarm in urban centres around the globe, exclusively in developing nations. The unrestrained urban expansion and subsequent industrialization, along with atypical population-boost, have magnetized environmental degradation as a burning concern for city planning [1]. After the liberalization in the 1990s, India has been incessantly

experiencing economic advancement, the rapid growth of the urban centres, uncontrolled infrastructural improvement, and industrial expansion [2]. According to the Central Pollution Control Board of India (CPCB), the major five constituents of air pollution are particulate matters (PM), nitrogen oxide, sulphur dioxide (SO₂), carbon monoxide (CO), and ozone (O₃) and, among them, the most prevalent threats for human health are PM₁₀ and PM_{2.5}. Since the ongoing decade, Indian metro cities have placed within the top 20 utmost polluted cities in the world exceeding the standard of specified air quality index (AQI) by the CPCB India and the World Health Organization (WHO) [3,4]. During 2015, in India, nearly one million lives were lost due to the high concentration of ambient PM [5].

Simultaneously, the environmental degradation vulnerability in the four megacities of India (Delhi, Kolkata, Mumbai, and Chennai) has increased, causing human health-related problems. According to the report (2016) of the World Health Organization (WHO) on the environmental performance index, Delhi is one of the most polluted cities of the world [6]. The revised environmental monitoring databases (from the year 2011 to 2016) among the largest megacities of 100 countries have listed Delhi on high rank in terms of PM₁₀ concentration [7]. A typical death due to the heat wave in Delhi reveals the importance of Land Surface Temperature (LST) as articulated by Mohan and Kandya [8]. The concentration of PM₁₀ in the city of Kolkata has exceeded the National Ambient Air Quality Standards (NAAQS) [9]. Changing patterns of the thermal environment, along with uncontrolled urbanization, are transforming vegetative lands into dry environments [10]. The satellite-based estimation of LST reveals a warming trend, i.e., average LST values range from 27.36 °C to 30.025 °C (from the year 1989–2006) and in 2010, it was 33.023 °C. Besides this, urban expansion has also reflected the impression on the alterations of other biophysical factors [10]. A similar trend in the ecological setup of the cities of Mumbai and Chennai can be found in studies of Kumar et al. (2016), Sundaram (2011), Partheeban et al. (2020), and Sathyakumar et al. (2020) [11–14].

Updated temporal and spatial information regarding environmental quality in the megacities of India could be the prerequisite to formulate new strategies to endorse further development. Urban Environmental Quality (UEQ) assessment depends on multidimensional aspects (spatial, physical, social, and economic traits of the city milieu) of the environment, which makes it more complex; this complex nature demands a comprehensive understanding of the environmental degradation process and its driving forces [15]. In this regard, one concerning issue is to determine the effective indicators of UEQ which may not only facilitate better mapping than can assist in city planning and sustainable growth as proficient management techniques. The remote-sensing-data-based Urban Environmental Quality (UEQ) assessment mainly provides information about land surface temperature, atmospheric elements such as air moisture and suspended particulate matters, vegetation status and biomass quantity, land use/land cover, and water [15]. Vegetation in the urban areas is a key variable to determine UEQ in several ways, i.e., freshening air through consuming CO₂, filtering sunlight and water, sieving pollutants, cooling heat influx, modifying local climatic setting, providing protection to animals and amusement field to society [16–20]. Land surface temperature (LST) is another foremost indicator of urban climate—controlling directly the comfortability and healthiness of urban environment, which is connected to the concept of urban heat island [15,21–23]. Various studies have regarded LST as an aspect of UEQ [24,25]. An exceeded standard amount of suspended particulate matters (PM₁₀ and PM_{2.5}) in the air is a high threat for public respiratory systems produced from industries, vehicles, dust, and residential energy [5,26]. Keeping in mind the importance of all these parameters for assessing Urban Environmental Quality Index (UEQI), this study considered five main elements which are mentioned in the literature, namely, PM₁₀ concentration, LST, NDVI, NDWI and NDMI. Although NDVI, NDWI, and NDMI are more or less stable in nature, aside from the undisturbed condition of the natural environment due to imposition of the lockdown phenomenon, these parameters may also change slightly, and, above all, these parameters are very important for assessing environmental quality [15,16,24,25].

COVID-19 is an extremely transmittable virus and was firstly originated in the Wuhan city of Central China during December 2019. Further, there have been outbreaks all over the world,

especially in various nations of Asia, Europe, and the United States of America. Up to 9 May 2020, globally 3,822,382 COVID-19 positive cases have been confirmed and 263,658 people have died according to WHO. In India, to date, 59,881 people have been infected and 1990 deaths by COVID-19 have been recorded (<https://www.covid19india.org/>). To break the infection chain in India, a nationwide lockdown was enforced from 24 March 2020 till 14 April 2020, and later it was extended a 2nd time till 17 May 2020. This lockdown was also imposed on all industrial sectors (excluding emergency service sectors) and on the mass transportation systems. Hence, the consequence of the biophysical environment has shown a drastic change. Sharma et al. (2020) reported that pollution status has been radically reduced across the 88 cities in India due to lockdown upshot as per the data provided by CPCB [27]. Following this, Mahato et al. (2020) suggested that short-term lockdown can be assumed to be an operative substitute scheme to be executed to control air pollution to preserve standard environmental quality [1].

Although some research has been done on the effect of the COVID-19 pandemic on ecology in various cities of India, very little or no studies could be found regarding the impact of the COVID-19 induced lockdown situation on the overall bio-physical Environmental Quality (EQ) of Indian cities. Researches have shown a more specific interest in air quality index (AQI) assessment based on station-wise monitored secondary nonspatial data. The present research is an effort to trace the effect of the COVID-19 pandemic on the alteration of the physical environment using satellite-image-derived PM₁₀ concentration, LST, NDVI, NDWI, and NDMI of the pre-lockdown period and during the lockdown period in four main big cities of India.

2. Study Area: Four Megacities of India

Four big cities of India, i.e., Mumbai, Delhi, Kolkata, and Chennai, were considered for assessing the impact of the COVID-19 induced lockdown situation on environmental quality. These four cities are strategically located in four different parts of India, playing a big role in the Indian economy (Figure 1). National Capital Territory (NCT) Delhi is the biggest Urban Agglomeration (UA) of India and the second most populated megacity of the world, with a population of 30.29 million [1] and with a population density of 11,297 people/sq. km. On the other hand, Mumbai is the ninth most populous megacity of the world, with a total population of 20.41 million. Mumbai is also ranked as one of the most polluted urban areas, having a 2.33 million vehicle count [11]. Kolkata has a total population of 14.85 million, which makes it the 16th largest megacity of the world, located in the eastern part of India. Chennai obtained the position of 30th most populated megacity of the world, with a population of 10.97 million. Due to intense emissions from vehicles, garbage, and biomass scorching, building construction, and natural space annihilation, the cities' ecological setups are under severe threat, and the environmental condition is gradually deteriorating for all four big cities, which are currently under investigation [8,28,29]. This increasing threat to the natural environment warrants an urgent assessment of the environmental quality during this dark time of the COVID-19 epidemic.

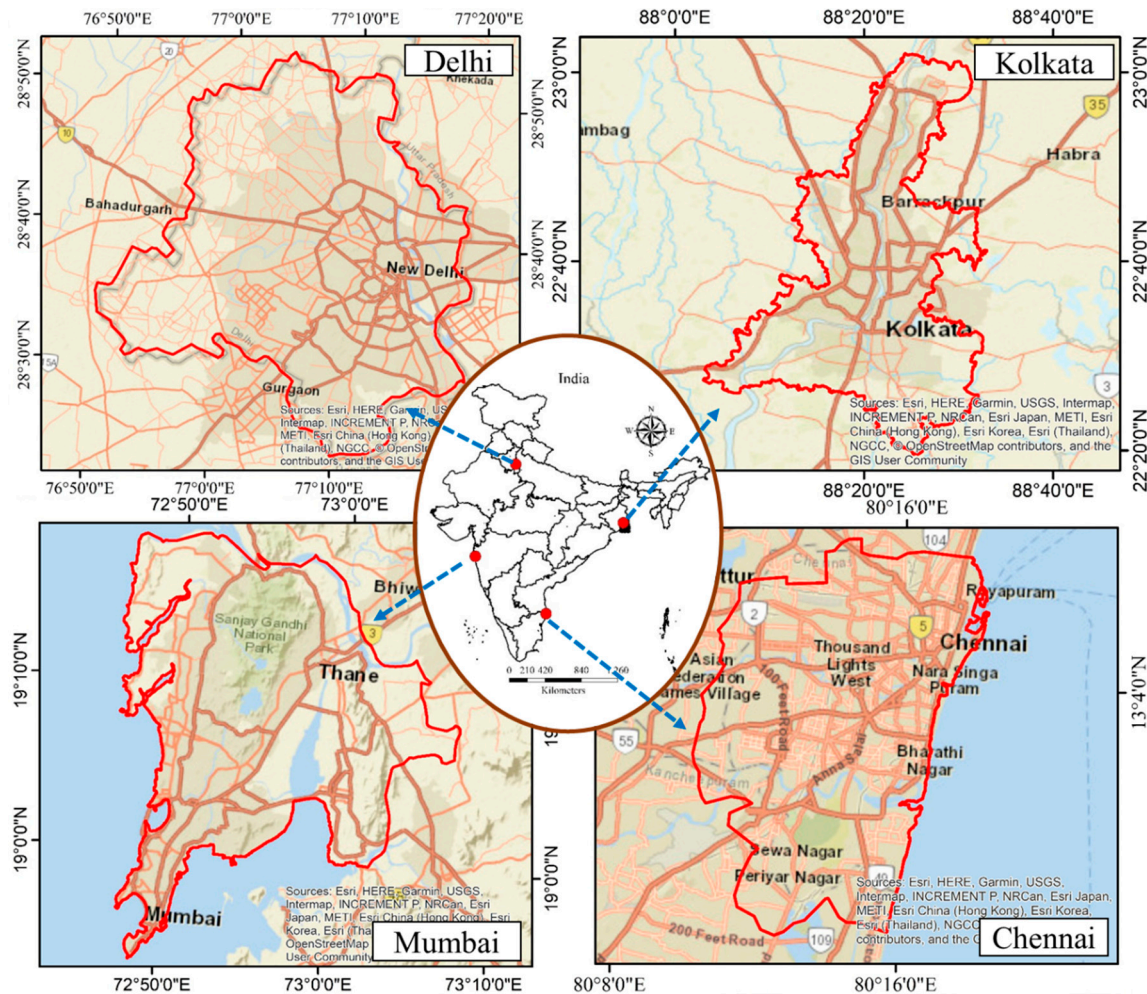


Figure 1. Location of the study areas.

3. Materials

Satellite Data

This research was performed using the satellite imageries which were downloaded from <https://landsat.usgs.gov/> (Table 1). Landsat 8 OLI (Operational Land Imager) and TIRS (Thermal Infrared Sensor) images covering the selected megacities for both pre-lockdown and during the lockdown period were collected for further exploration. Landsat 8 satellites with two sensors, i.e., OLI (Operational Land Imager) and TIRS (Thermal Infrared Sensor), are comprised of nine spectral and two thermal bands. Spectral bands have a spatial resolution of 30 m, except the band 8 (panchromatic band of 15 m spatial resolution) and TIRS bands are attained at 100 m spatial resolution, though resampled into 30 m for the end user (Table 2).

Table 1. Corresponding dates, image ID, and other properties of satellite images for each of the megacities.

Study Area	Date	Sensor	Image ID	% of Cloud	Remarks
Mumbai	Same time of pre-lockdown, 2019	10\04\2019	LC08_L1TP_148047_20190410_20190422_01_T1	0.72	No cloud cover on the study area
	Pre-lockdown, 2020	11\03\2020	LC08_L1TP_148047_20200311_20200325_01_T1	5.77	7.29% on land but very less on the study area
	During lockdown, 2020	12\04\2020	LC08_L1TP_148047_20200412_20200422_01_T1	1.62	No cloud cover on the study area
Delhi	Same time of pre-lockdown, 2019	28\04\2019	LC08_L1TP_146040_20190428_20190508_01_T1	0	No cloud cover on the study area
	Pre-lockdown, 2020	13\03\2020	LC08_L1TP_146040_20200313_20200325_01_T1	34.4	No cloud cover on the study area
	During lockdown, 2020	29\03\2020	LC08_L1TP_146040_20200329_20200409_01_T1	0.03	No cloud cover on the study area
Kolkata	Same time of pre-lockdown, 2019	20\04\2019	LC08_L1TP_138044_20190420_20190507_01_T1	18.64	No cloud cover on the study area
	Pre-lockdown, 2020	21\03\2020	LC08_L1TP_138044_20200321_20200326_01_T1	32.57	No cloud cover on the study area
	During lockdown, 2020	06\04\2020	LC08_L1TP_138044_20200406_20200410_01_T1	0.58	No cloud cover on the study area
Chennai	Same time of pre-lockdown, 2019	31\03\2019	LC08_L1TP_142051_20190331_20190404_01_T1	2.46	No cloud cover on the study area
	Pre-lockdown, 2020	17\03\2020	LC08_L1TP_142051_20200317_20200326_01_T1	3.54	No cloud cover on the study area
	During lockdown, 2020	02\04\2020	LC08_L1TP_142051_20200402_20200410_01_T1	0.28	No cloud cover on the study area

Table 2. Band details of the satellite imagery used in this study.

Band	Band Description	
	Spectral Resolution (μm)	Spatial Resolution (m)
Band 1-Coastal/Aerosol	0.433 to 0.453	30
Band 2-Visible blue (BLUE)	0.450 to 0.515	30
Band 3-Visible green (GREEN)	0.525 to 0.600	30
Band 4-Visible red (RED)	0.630 to 0.680	30
Band 5-Near-infrared (NIR)	0.845 to 0.885	30
Band 6-Short wavelength infrared1 (SWIR1)	1.56 to 1.66	30
Band 7-Short wavelength infrared2 (SWIR2)	2.10 to 2.30	30
Band 8-Panchromatic	0.50 to 0.68	15
Band 9-Cirrus	1.36 to 1.39	30
Band 10-Thermal Infrared (TIRS) 1	10.3 to 11.3	100 * (30)
Band 11-Thermal Infrared (TIRS) 2	11.5 to 12.5	100 * (30)

* represents the original spatial resolution of the bands 10 and 11 of TIRS 1 and 2.

4. Methodology

The present research was completed using the steps mentioned in Figure 2.

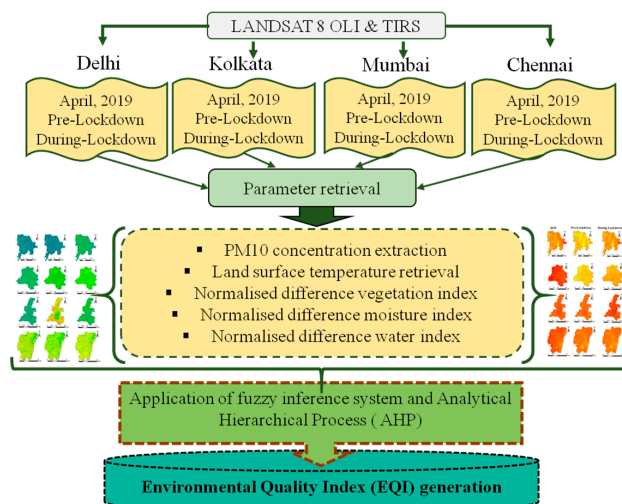


Figure 2. Workflow diagram of the present research.

4.1. PM₁₀ Concentration

The concentration of PM₁₀ is an important element for air quality, but these important air quality parameter data are not available sufficiently for Indian cities. Lesser number of observation points are available which can be used for interpolation to get a spatial variation of PM₁₀ concentration with a smaller spatial unit. This problem of PM₁₀ concentration assessment can be minimized through the integration of satellite-derived images and ground observation data. The entire process of PM₁₀ concentration extraction is discussed below.

4.1.1. Conversion from DN Value to Top of the Atmosphere (TOA) Reflectance

The digital number (DN) value of a satellite band is the converted representation of actual reflectance from the surface. This converted reflectance value should be transformed into actual reflectance value for measuring the actual amount of reflectance from the land surface. The DN value for band 1 to 4 of Landsat 8 is converted into Top of Atmosphere value using Equation (1).

$$p\lambda' = M\rho Qcal + Ap \tag{1}$$

where

$p\lambda'$ = Top of Atmosphere planetary reflectance, without solar angle correction,

$M\rho$ = Multiplicative rescaling factor for a specific band (REFLECTANCE_MULT_BAND_x, where x indicates band number),

$A\rho$ = Additive rescaling factor for a specific band (REFLECTANCE_ADD_BAND_x, where x indicates band number),

$Qcal$ = Converted pixel values (DN value).

4.1.2. Sun Angle Correction

TOA reflectance is a solar angle uncorrected product which may have some deviated value due to changes in solar angle; that is why solar angle correction is important. This solar angle correction of TOA data is performed using Equation (2).

$$p\lambda = \frac{p\lambda'}{\cos(\Theta SZ)} = \frac{p\lambda'}{\sin(\Theta SE)} \quad (2)$$

$\rho\lambda$ = Solar angle corrected Top of Atmosphere planetary reflectance.

$p\lambda'$ = Without solar angle corrected Top of Atmosphere planetary reflectance.

ΘSE = Sun elevation angle (Local) (SUN_ELEVATION data found in the metadata section).

ΘSZ = Solar zenith angle (Local); [$\Theta SZ = 90^\circ - \Theta SE$].

More accurate reflection calculation depends on per-pixel solar angle data, which are not correctly available with Landsat 8 image metadata, which is substantiated with the scene centre solar angle value [30].

4.1.3. Regression Analysis and PM₁₀ Concentration Calculation

Correlation among ground-measured PM₁₀ concentration and difference between TOA reflectance and sun angle corrected TOA reflection represents the amount of PM₁₀ concentration for a pixel. Least-root-mean-square error (RMSE) value and higher R² value among all possible combinations of the band between band 1 to band 4 of Landsat 8 satellite image were selected to obtain multiplicative and additive coefficient value, which is used to calculate actual PM₁₀ concentration value for each pixel with the help of sparsely distributed PM₁₀ concentration observation points located within the studied four megacity areas.

4.2. LST Retrieval

The steps to extract the LST from the thermal band of the satellite images are as follows:

4.2.1. Digital Number to Spectral Radiance Conversion

Following the law of electromagnetic radiation of the objects (each object radiates Electromagnetic Radiation (EMR), as each has temperature more than absolute zero (K)), at-sensor radiance can be achieved through the conversion of recognized signals by the Thermal Infrared Sensor (TIRS) and Enhanced Thematic Mapper (ETM+). Spectral radiance ($L\lambda$) was computed by the formula given below [31]:

$$L\lambda = \text{“gain”} * QCAL + \text{“offset”} \quad (3)$$

where gain = radiance slope/DN transformation function; DN signifies digital number of a specific pixel; bias is the radiance intercept/DN transformation function. It may also express as:

$$L\lambda = LMIN\lambda + [(LMAX\lambda - LMIN\lambda) / (QCALMAX - QCALMIN)] * QCAL \quad (4)$$

where $QCAL = DN$ of pixels; $QCALMAX = 255$; $QCALMIN = 0$; $LMIN\lambda =$ spectral radiance for thermal band at $DN = 0$, and $LMAX\lambda =$ spectral radiance for thermal band at $DN = 255$. Replacement of the corresponding values in Equation (3) provides a simpler Equation (4):

$$L\lambda = (0.037059 \times DN) + 3.2 \quad (5)$$

4.2.2. Spectral Radiance to At-Satellite Brightness Temperatures

Based on the category of land cover, rectifications for emissivity (ϵ) were done for the radiant temperatures. Generally, vegetation areas have assigned with 0.95 and non-vegetation areas have assigned with a value of 0.92, following Nichol [32]. Emissivity-corrected LST was figured ensuing Artis and Carnahan [33].

$$T_B = \frac{K_2}{\ln\left(\frac{K_1}{L_\lambda} + 1\right)} \quad (6)$$

where L_λ is Spectral Radiance in $W \cdot m^{-2} \cdot sr^{-1} \cdot \mu m^{-1}$ and K_1 and K_2 are two constants of two pre-launch calibrations.

4.2.3. LST Estimation

The values of temperature attained from the above computations are denoted to a black body. Hence, it requires rectification of spectral emissivity (ϵ). It can be performed rendering to the type of land cover or by accomplishing corresponding emissivity values from the NDVI values for respective pixels [34]. The method of emissivity-rectified LST formulation can be stated as the equation below [33]:

$$LST = T_B / [1 + \{(\lambda \times T_B / \rho) \times \ln \epsilon\}] \quad (7)$$

Here, LST = Land Surface Temperature in Kelvin, $T_B =$ At-sensor brightness temperature, $\lambda =$ TOA reflectance, $\ln \epsilon =$ Emissivity.

$$\text{Land surface emissivity } (\epsilon) = 0.004 \times P_v + 0.986 \quad (8)$$

where P_v is the proportion of vegetation which can be set up as:

$$P_v = \left(\frac{NDVI_{j_r} - NDVI_{\min}}{NDVI_{\max} - NDVI_{\min}} \right)^2 \quad (9)$$

4.2.4. Kelvin to Degree Celsius Conversion

To simplify the conception, the measuring unit of these derived LSTs was transformed from a Kelvin scale to degree Celsius scale, applying the formula $0^\circ C$ equal to 273.15 K.

4.3. Biophysical Indices Extraction

To assess the instant changes of Environmental Quality Index (EQI) in the present framework of research, the three most relevant biophysical parameters have been included, such as Normalised Difference Moisture Index (NDMI), Normalised Difference Vegetation Index (NDVI) and Normalised Difference Water Index (NDWI) [15]. NDWI designates the vegetation water content and the status of vegetation can appositely represent by combining it with NDVI [35]. This indicator is the combination of reflectance of green plants, dry and plant absent areas, and soil parts through two near-infrared (NIR) bands [36]. It is computed using Equation (10).

$$NDWI = (NIR - SWIR) / (NIR + SWIR) \quad (10)$$

where index values near to the 1 signify water bodies, to -1 signify dry land and close to 0 denotes moderately humid lands [37].

NDVI is the most widely considered variable to extract vegetation information, i.e., health status and spatial distribution, etc., in a region that was derived following Equation (11) [38].

$$NDVI = (NIR - RED) / (NIR + RED) \quad (11)$$

where NIR and RED are the near-infrared band and red band respectively. The value ranges from $+1$ to -1 , signifying vegetated zone to bare lands, and value near to 0 epitomizes grasslands [39].

NDMI was used to estimate the humidity contents of various landscape features such as soils, rocks, and plants. Eco-environmental exposure could be estimated using NDMI [39]. This was computed following Jin and Sader [40].

$$NDMI = (NIR - IR) / (NIR + IR) \quad (12)$$

where IR is the infrared. A high amount of humidity designated by NDMI values > 0.1 and values near to -1 signifies a low humidity level.

4.4. Fuzzy Inference System (FIS)

FIS is a proficient methodical approach to draw inferences using a set of input variables [41]. Fuzzy logic has great acceptance as a multi-criterion-based decision-making process has been adopted in various fields [42,43]. A precise result can be obtained using this method, because it assigns different membership grades for definite pixels and maximizes the membership degrees to attain destiny [43,44].

The fuzzy Mamdani system involves human's empirical knowledge to make an inference according to the input variable [45]. This approach is operated through fuzzification of the input variable layers, rule assessment, fuzzy end inference, and defuzzification [46,47]. To achieve the goal, FIS need the following setup:

Fuzzy Model Setup

The framework of this model for this research was built upon the following two heads:

- (a) Fuzzy membership function was applied to five Environmental Quality Variables (EQV) considering their influence on urban environment.
- (b) Positioning Control Point (CP) in order to find out the most influential range of the five EQVs to produce Environmental Quality Index (EQI).

Membership function to each EQV was dispensed to produce a normalized fuzzy layer of each raw variable, and CP for each was also specified according to the distributional characteristics of them. This two-phase operation ensured the conversion of each EQV layer into a 0–1 value range of pixels to make the data unidimensional, which is the most acceptable approach to overlay different layers with dissimilar units [41]. Fuzzy membership with monotonically decreasing function allotted to those EQVs which influence level gradually decreases following sigmoidal curve from CP 'a' to 'b' or CP 'c' to 'd' concerning Environmental Quality Index (EQI) determination (Table 3). Whereas, monotonically increasing membership function signifies the vice versa aiming the same goal (Table 3). Membership function and shape of EQVs and corresponding CP has been enlisted in Table 3.

$$\mu = \frac{1}{\left\{1 + \left(\frac{x-c_1}{c_2-c_1}\right)^2\right\}} \quad (13)$$

where μ is the standardized score of an EQV, x signifies raw score, and c_1 and c_2 are base and end value of control point, respectively. To optimize the decision space, c_1 and c_2 were used.

$$\mu_d(x_n) = \exp\left(\frac{(x_n - v_n)^2}{2S_n^2}\right) \tag{14}$$

Table 3. Control point, fuzzy membership function and shape determination for fuzzy transformation of the Environmental Quality Value (EQVs).

EQVs	Control Points				Fuzzy Membership Function	Fuzzy Membership Shape
	a	b	c	d		
PM ₁₀ concentration	1	281			Monotonically increasing	Sigmoidal
LST	7	50			Monotonically increasing	Sigmoidal
NDVI			-0.13	0.65	Monotonically Decreasing	Sigmoidal
NDWI			-0.57	0.56	Monotonically Decreasing	Sigmoidal
NDMI			-0.65	0.55	Monotonically Decreasing	Sigmoidal

Equation (14) is used to set fuzzy rules, i.e., for a fuzzy set, resultant of all the inputs of S rules, fuzzy set $\mu_e(S)$, where s fit in ‘S’ with different decisions of agent X, which can be inscribed as the equation below:

$$\mu_{E(X)} = \bigoplus_1^s \mu_{e(s)} \tag{15}$$

In the present research, monotonically increasing fuzzy membership function with sigmoid pattern distribution curve was assigned for the parameters PM₁₀ concentration in the air and land surface temperature as the degradation risk of EQI increases with the increasing value of these two parameters within the specified CP range (Table 3). Similarly, for the NDVI, NDWI, and NDMI, the fuzzy membership shape was assigned following the same, but membership function type was followed as monotonically decreasing which means that, as the value of these indices increases, the probability of environmental degradation decreases.

4.5. Fuzzy-Analytical Hierarchical Process (AHP)

For modeling, computation of the weights of each parameter is essential to produce the goal. AHP, in this regard, is an efficient method to obtain weights of the inducing parameters to make decisions in complex problems [48]. The method involves making a comparison among the input parameters based on their relative importance to target decision through forming a pairwise comparison matrix [48,49], which enable to compute the parameter weights [47,50]. The stepwise process of the AHP method includes a breakdown of the complex structure of the problem into different alternatives and criteria, i.e., EQVs in here, assignment of preference values to the alternatives or criteria according to the scale of importance considering their association with the goal, i.e., EQI in this research [48,51], and computation of the weights following Satty [48]. The corresponding parameter weights are computed by dividing the cell values by values of the column sum of the pairwise comparison matrix. The importance scale for the parameter in respect of EQI was determined and assigned following the earlier studies, the appearance of the study area, and experts’ opinions involved in this field [52,53]. Further progression was enabled through calibration of the pairwise comparison matrix and validated by the rule of Consistency Ratio (CR), which reflects the trustworthiness and applicability of the analysis performed. A value of <0.1 of CR suggests the reliability of the analysis. The pairwise comparison matrix, consistency ratio, and relative weights of the parameters in the present analysis are enlisted in Table 4. Pairwise comparison matrix and CR can be expressed using the equations below.

$$A = \begin{matrix} & a_{11} & a_{12} & a_{13} & a_{1n} \\ & a_{21} & a_{22} & a_{23} & a_{2n} \\ & \dots & \dots & a_{ij} & \dots\dots \\ a_{n1} & a_{n2} & a_{n3} & a_{nn} \end{matrix} \tag{16}$$

where

$$a_{ij} = \frac{W_i}{W_j} = \frac{\text{weight for attribute } i}{\text{weight for attribute } j} \quad (17)$$

Table 4. Pairwise comparison matrix for considered EQVs to derive relative weight using the Fuzzy-Analytical Hierarchical Process (AHP) method.

	PM ₁₀	LST	NDVI	NDWI	NDMI
PM ₁₀	1				
LST	0.33	1			
NDVI	0.20	0.20	1		
NDWI	0.14	0.14	0.33	1	
NDMI	0.11	0.11	0.20	0.33	1
Consistency Ratio is 0.07					

The computation of *CR* can be expressed as

$$CR = CI/RI \quad (18)$$

where *CI* and *RI* are the consistency index and random index, respectively, and *CI* can be expressed as the equation below:

$$CI = \frac{\lambda_{Max} - n}{n - 1} \quad (19)$$

where λ_{Max} = largest eigenvalue, and *n* = order of the matrix.

In this research, fuzzy-AHP was the process of a fuzzy behavioural structure where the fuzzy-transformed layer of the EQVs was weighted (Table 5) by the AHP method with respect to their influence to estimate dynamics status of environmental quality status in three different phases.

Table 5. Relative weight for each EQV generated through the AHP method for using in the weighted linear combination overlay method to generate the final vulnerable area map.

EQVs	Weightage
PM ₁₀ concentration	0.492
Land Surface Temperature	0.3136
NDVI	0.1093
NDWI	0.0553
NDMI	0.0298

4.6. EQI Generation

After assigning the weights to the fuzzy-converted layers of EQVs, to produce the EQI maps of four megacities of India, the layers were integrated using the Linear Combination (LCM) overlay technique as each parameter was unidirectional and unit-less. The LCM was performed following Equation (20).

$$LCM = \frac{1}{n} \times \sum_{i=1}^n D_i \times w_i \quad (20)$$

where *n* is the number of parameters considered, w_i is the weight of *i* parameter, and *D* is the decisive EQV.

5. Results

5.1. Changing Patterns of PM₁₀ Concentration

PM₁₀ concentration is one of the determinants of air quality as well as environmental quality. Mainly, industrial activities, motor vehicles, and construction works are the sources of PM₁₀ concentration in the air which may destroy human comforts and creates lots of respiratory diseases.

This is not only the direct human problem, but it also harms environmental conditions indirectly in the form of increasing air and land surface temperature. The lockdown situation has successfully restricted the spread of the COVID-19 virus in the study areas. These restrictions play a positive role in recovering the past situation of PM_{10} concentration by reducing PM_{10} supply into the atmosphere. Figure 3 indicates a clear declination of PM_{10} concentration from 2019—the same month for which lockdown data are collected to 2020 lockdown, representing the same period, although the pre-lockdown phase shows an increasing amount of PM_{10} concentration compared to 2019, which is a natural trend of increasing this air quality parameter. This situation is applicable for Mumbai and Chennai, whereas a different situation is observed for Delhi and Kolkata. The PM_{10} concentration map of Delhi shows that the pre-lockdown phase indicated a decreased amount of PM_{10} concentration, but lockdown time indicated a higher decrease in PM_{10} concentration than in 2019 and the pre-lockdown situation. This different result has taken place as a result of the early shutdown of the industrial sector and restriction on human movement before imposing lockdown in India. Kolkata is showing an exceptional pattern of PM_{10} concentration compared to the rest of the study sites, because the pre-lockdown phase showing minimum PM_{10} concentration than 2019 and lockdown phase, although the lockdown phase representing lower PM_{10} concentration than 2019 same month. This is maybe the same reason as in Delhi, which is discussed earlier.

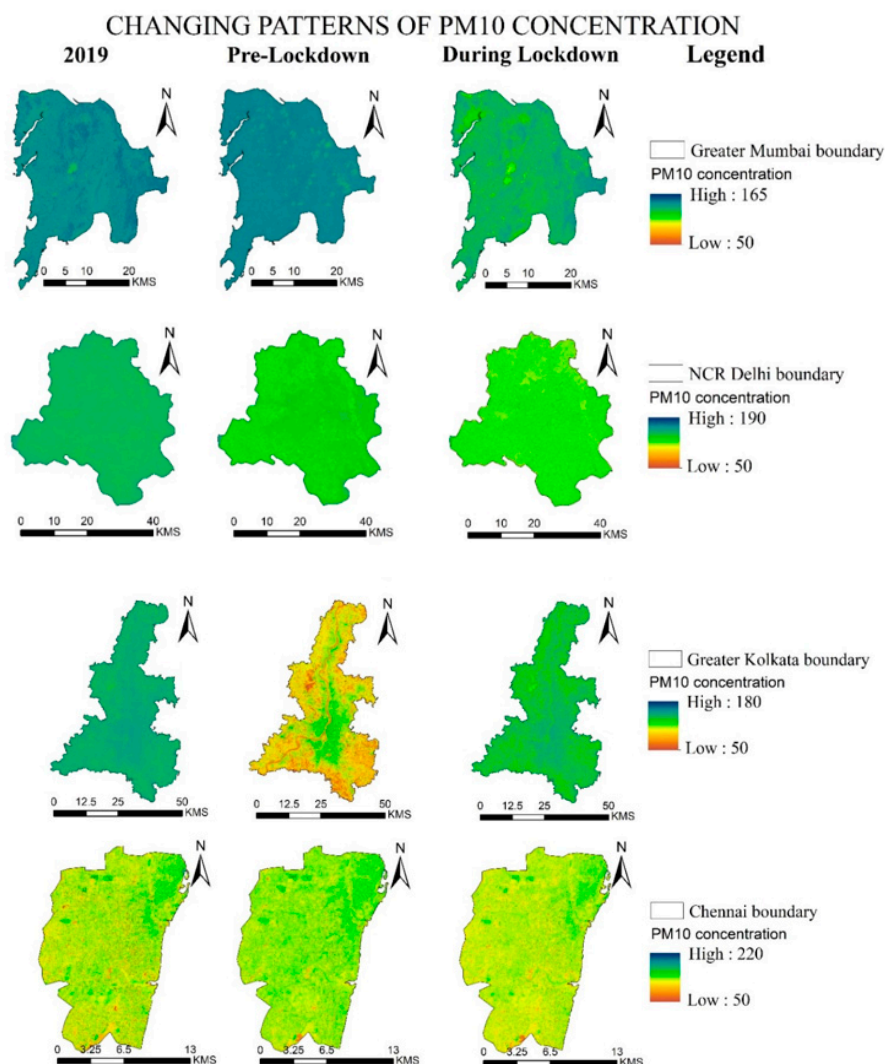


Figure 3. Changing pattern of PM_{10} concentration in four megacities of India during the same season in 2019 of the pre-lockdown 2020; pre-lockdown, 2020 and during the lockdown, 2020.

5.2. Changing Patterns of LST

LST is also an important parameter for environmental health, which depends on a large number of atmospheric and physical factors. The month of the study, cloudy condition, Land Use/Land Cover (LULC) patterns, and many more factors govern the patterns of LST for an area. To avoid the problems of different seasons and months, a similar month satellite image was collected with less than 10% cloud coverage. On the other hand, LULC pattern has become constant from pre-lockdown to lockdown time, although LULC patterns from 2019 to 2020 lockdown time have changed as a natural process. For this reason, LULC is not considered for assessing environmental quality.

Land Surface Temperature indicates an increasing trend over time due to LULC change and other global phenomena. LST maps indicate that 2019 and lockdown time is higher than pre-lockdown, which is a natural phenomenon due to the changes in study months; 2019 and lockdown time data were collected for the last week of March and the first two weeks of April, which generally represents higher temperature months than pre-lockdown data collected during the period of February last week to March second week. Here in India, February and March represent the transition period between the winter and summer season, whereas March last to April represents the summer season, which indicates a general trend of temperature increase. Mumbai, Delhi, and Kolkata are showing a higher temperature of 48 °C to 50 °C for 2019, pre-lockdown, and lockdown time, whereas Chennai is showing a lower high temperature of 42 °C (Figure 4). On the other hand, both of these four study areas are showing a similar trend of LST patterns; same time of lockdown in 2019 and lockdown time showing a higher temperature than pre-lockdown time.

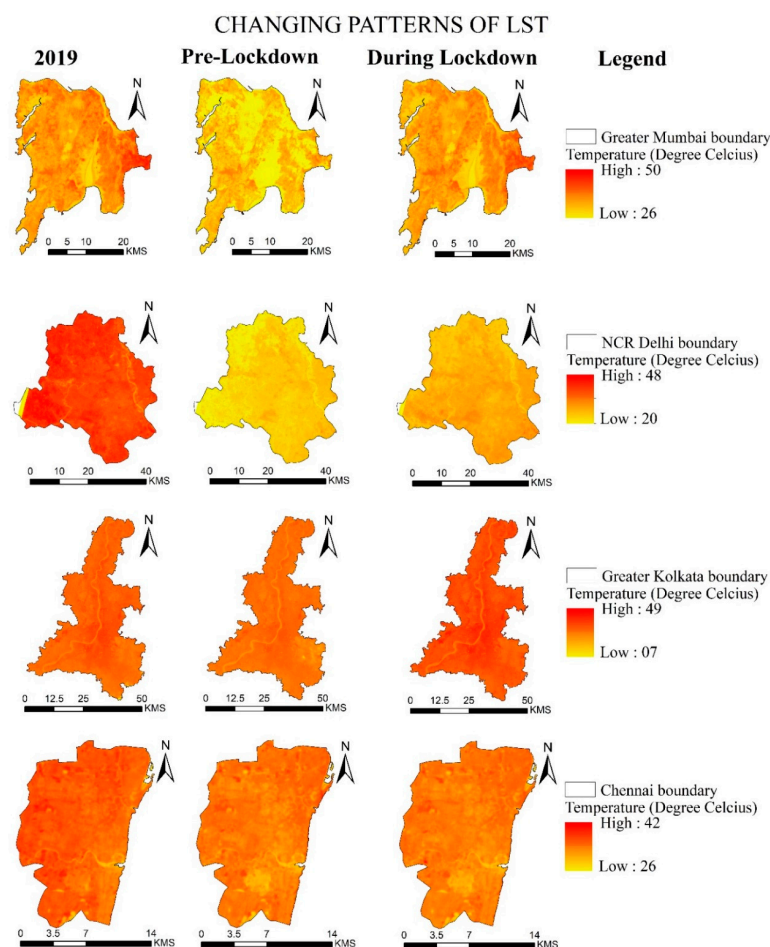


Figure 4. Changing pattern of land surface temperature in four megacities of India during the same season in 2019 of the pre-lockdown 2020, pre-lockdown, 2020, and during the lockdown, 2020.

5.3. Changing Patterns of Biophysical Indices

Bio-physical indices are calculated from remotely sensed satellite images to quantify the changing nature of some environmental parameters which may determine the quality of the environment for an area. Previous studies have used various bio-physical indices to assess the nature of environmental conditions and their changing nature such as NDVI, NDWI, NDBI, and NDMI. For this study, three biophysical indices were calculated from satellite images for each phase for all the study areas to assess the changing patterns of bio-physical environmental quality for the study time. Normalized Difference Vegetation Index (NDVI) represents the greenness of an area and positive greenness indicates a healthy environmental condition. The greenness of the study areas has increased from 2019 and pre-lockdown condition to lockdown condition due to the restriction of human movement and undisturbed condition of the existing natural vegetation. On the other hand, the emergence of newly vegetated areas in previously open spaces results in a high level of greenness during this time. This situation is also applicable to all megacities, which is a positive indication from the perspective of positive environmental health. Normalized Difference Water Index (NDWI) is also a positive indication of environmental health. Patterns of NDWI in the study areas are ranging between -0.55 and 0.32 for Mumbai, -0.55 and 0.54 in Delhi, -0.56 and 0.31 in Kolkata and -0.53 and 0.32 in Chennai, all of these ranges indicating that amounts of wetness in the study areas are not so high for any time period of this study (Figure 5). The presence of the water body or volume of wetness is important for maintaining a healthy environment. The overall analysis found that, for Mumbai, Delhi, and Chennai, NDWI value has increased during pre-lockdown time than in 2019 and lockdown time, but exceptionally Kolkata is showing a different condition with higher NDWI value during lockdown time (Figure 6).

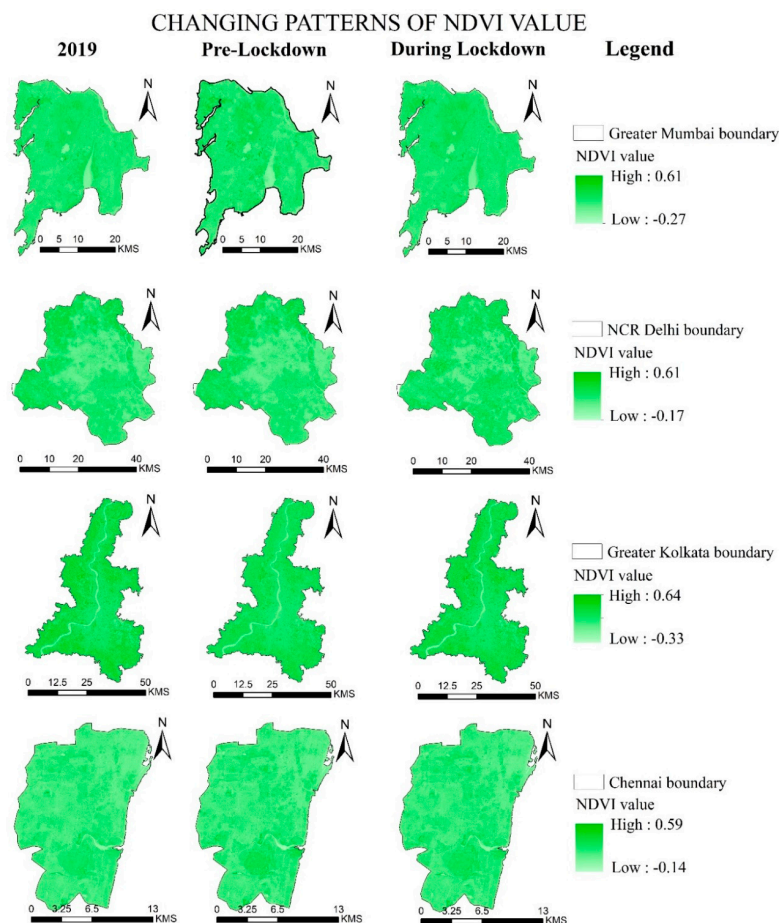


Figure 5. Changing pattern of NDVI in four megacities of India during the same season in 2019 of the pre-lockdown 2020, pre-lockdown, 2020 and during the lockdown, 2020.

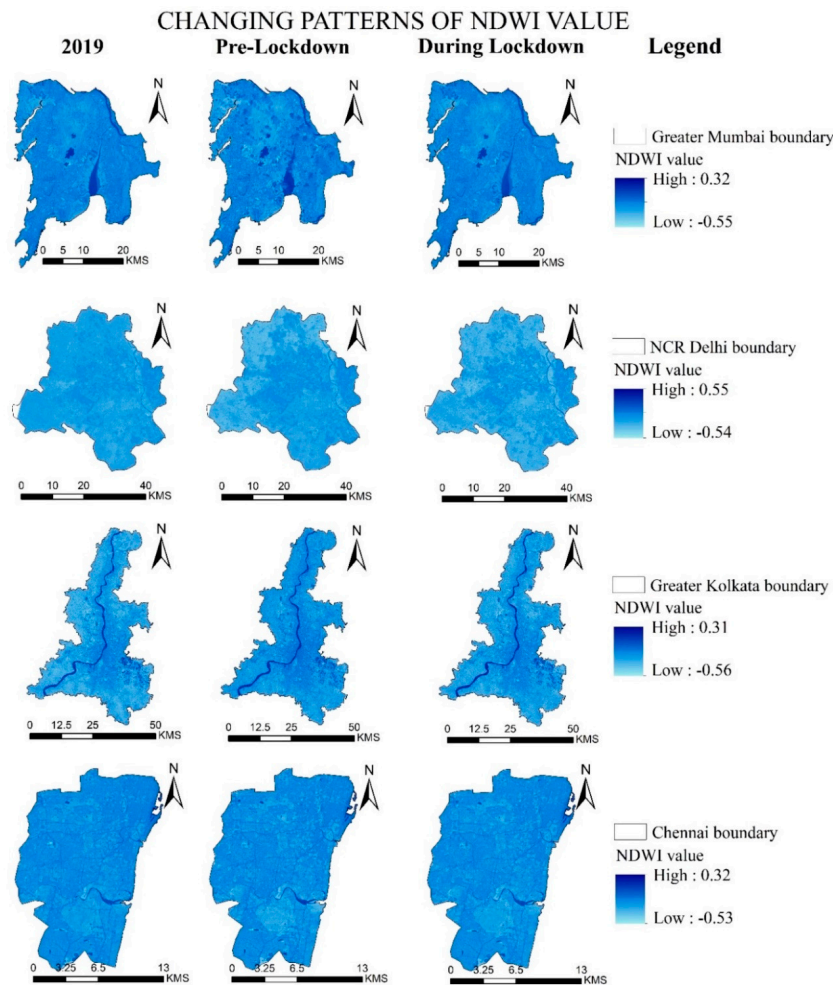


Figure 6. Changing pattern of NDWI in four megacities of India during the same season in 2019 of the pre-lockdown 2020, pre-lockdown, 2020 and during the lockdown, 2020.

Normalized Difference Moisture Index (NDMI) represents the amount of moisture content in the surface, which also determines the environmental condition of an area. Less human intervention results in an increase in NDMI value as human intervention alters the nature of moisture availability. NDMI index values for the study areas are indicating that NDMI value has increased during lockdown time than in 2019 and pre-lockdown time for Mumbai, Kolkata, and Chennai, where Delhi has to gain more moisture condition in pre-lockdown time than in 2019 and lockdown time (Figure 7). This may be due to the atmospheric condition of the Delhi area during the internment of satellite data.

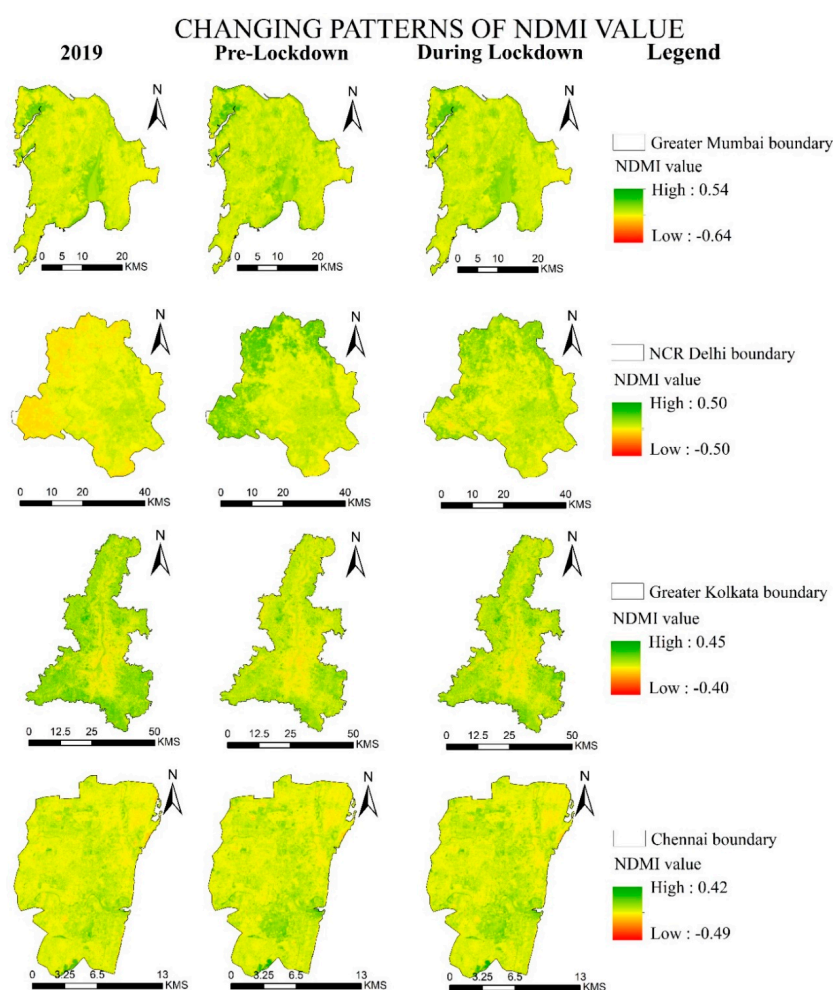


Figure 7. Changing pattern of NDMI in four megacities of India during the same season in 2019 of the pre-lockdown 2020, pre-lockdown, 2020 and during the lockdown, 2020.

5.4. Impact of COVID-19 Lockdown on Environmental Quality

Published articles on COVID-19 impact the environment, indicating that different environmental parameters, especially air quality parameters, have changed positively due to the lockdown situation in the whole world. India is not an exception, because India also started lockdown from 24 March 2020 for the whole country. A positive effect on air quality and some aspects of the physical environment is already notified by some researchers, but none of the studies assessed overall environmental quality for any part of the country. Indian megacities are the worst COVID-19 affected areas that were strictly following the lockdown conditions from the beginning, which resulted in the improved environmental quality of the studied megacities. It is found from this study that environmental quality has improved from the same month of 2019 to the same lockdown month. The general trend of environmental quality of the studied cities is degraded from its previous years due to the increase of human intervention [10]. According to this trend, the lockdown time of 2020 should have a higher environmental degradation than the same month of 2019, but this study shows that environmental quality has improved in 2020 compared with the same month of 2019, which has shown a positive indication from the perspective of environmental quality. This positive indication is a hope of light in the darkness of the COVID-19 situation. Figure 8 indicates that environmental quality has improved from 2019 to 2020 for Mumbai, Delhi, and Chennai, although pre-lockdown time shows a better environmental quality for all three study areas except Chennai, due to the change in the month, which represents low-temperature months compared with lockdown month. This stated result is also visible

from Figure 9, which shows the changing patterns of physical environmental quality in five classes, divided using Jenkin's Natural Break classification system with similar class range values to make it comparable between time and study sites. Areal change of different environmental quality index classes show that very low degraded environmental quality area is increased from 10.22% in 2019 to 38.45% in 2020 for Mumbai with the same month data for both years. This fact is also true for the other three study sites of Delhi, and Chennai with a changing value from 2019 to 2020, as 1.50% to 71.03% and 58.38% to 59.95%, respectively (Table 6). On the other hand, Kolkata is indicating an increasing low environmental degraded area from 52.16% in 2019 to 35.75% in lockdown time (Figure 10). Similarly, low environmental degradation areas have also increased in the lockdown period (percentage) in Mumbai, Delhi, Kolkata, and Chennai, respectively, from 2019 to 2020 (Table 6). The very high environmental quality degradation area has decreased for three studied megacities, except for Kolkata, which is also the same for high environmental quality degradation areas for three megacities, except for Chennai and Kolkata. The overall environmental quality degradation index has improved from 2019 to lockdown time, which is a positive indication for the whole world in the era of urbanization and environmental change.

Table 6. Pattern of environmental quality degradation in four megacities of India.

Study Area	Date	Very Low	Low	Medium	High	Very High
Mumbai	2019	10.22759	19.97495	35.34755	21.62421	12.8257
	Pre-lockdown	46.19468	32.35018	18.56851	2.787521	0.099114
	Lockdown	38.44749	31.63997	22.3983	5.484552	2.029686
Delhi	2019	1.502448	1.08621	8.639542	30.67348	58.09832
	Pre-lockdown	94.39192	5.593551	0.0135	0.0004	0.000629
	Lockdown	71.02876	27.36464	1.565073	0.040099	0.00143
Kolkata	2019	52.16253	25.94085	16.33086	4.490782	1.074978
	Pre-lockdown	55.86787	37.05701	7.02363	0.019139	0.032355
	Lockdown	35.74941	31.45045	20.39915	8.486124	3.914865
Chennai	2019	58.38214	28.33292	12.44535	0.463332	0.376257
	Pre-lockdown	44.20491	37.07574	16.24046	1.987608	0.491288
	Lockdown	59.94629	31.48092	7.667207	0.740598	0.164985

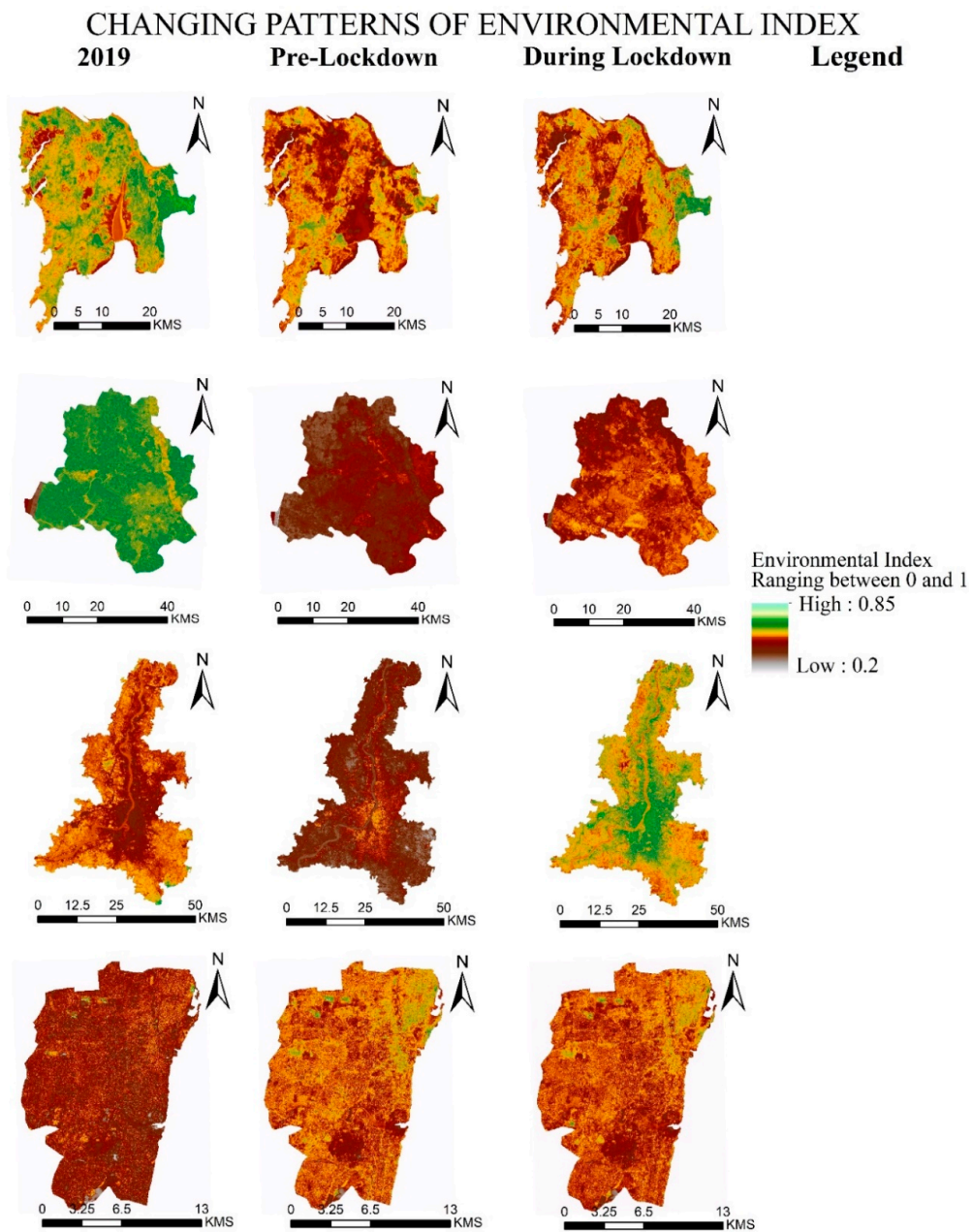


Figure 8. Changing pattern of the environmental quality index in four megacities of India during the same season in 2019 of the pre-lockdown 2020, pre-lockdown, 2020 and during the lockdown, 2020.

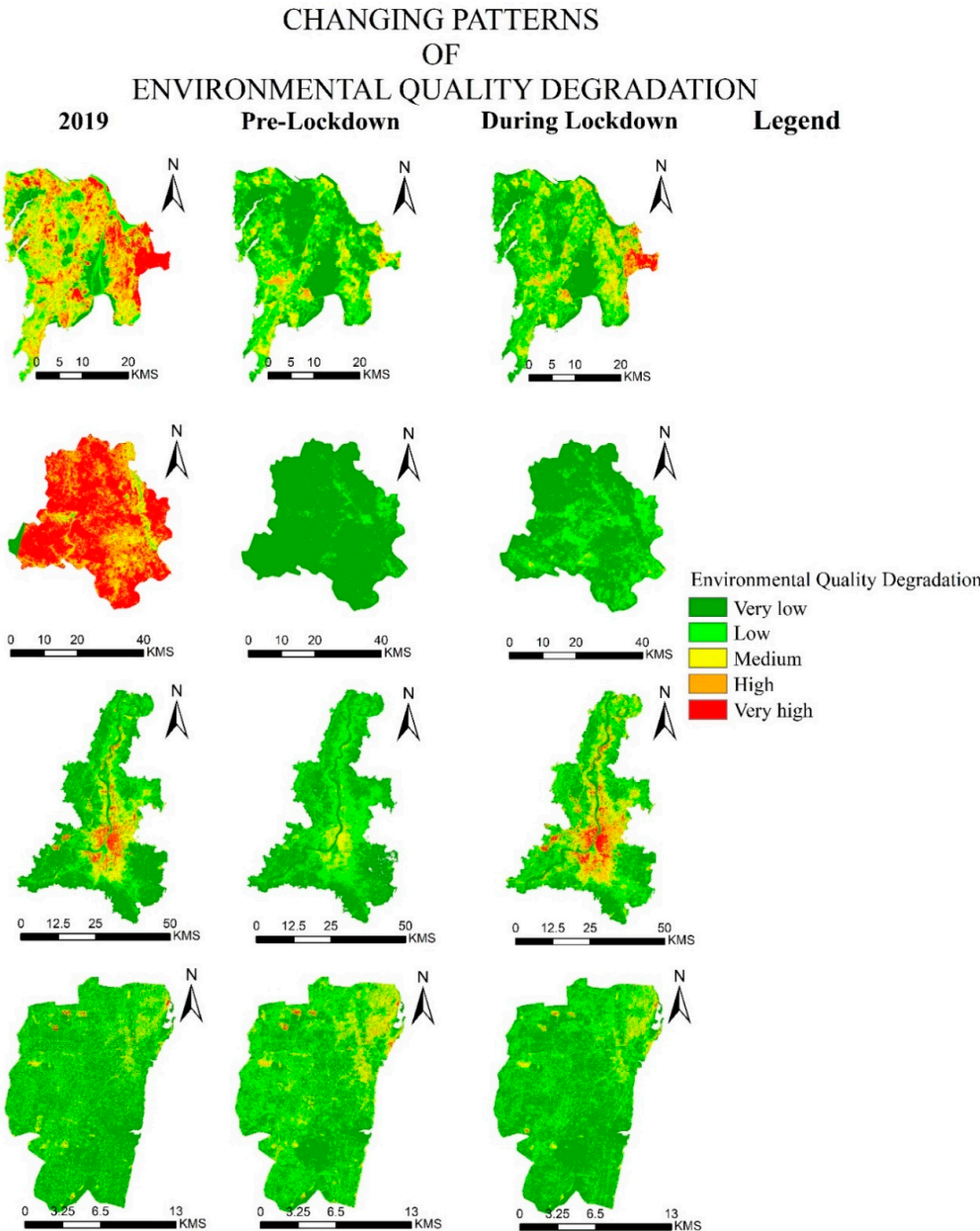


Figure 9. Spatial distribution of environmental quality vulnerability in four megacities of India during the same season in 2019 of the pre-lockdown 2020, pre-lockdown, 2020 and during the lockdown, 2020.

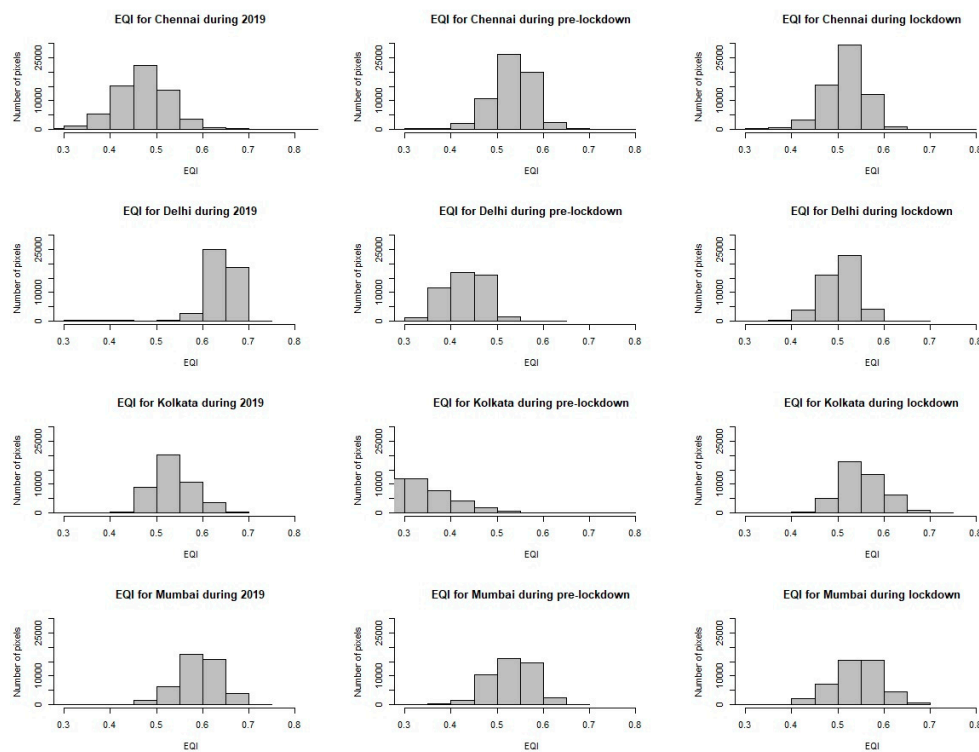


Figure 10. Changing pattern of Environmental Quality Index (EQI) in four megacities of India during the same season in 2019 of the lockdown 2020, pre-lockdown, 2020 and during the lockdown, 2020.

6. Discussion

Environmental quality for the world has changed negatively for the last few decades due to rapid population growth and increased human intervention in the natural environment; more specifically, physical environmental parameters have changed rapidly such as air quality, water quality, land surface temperature, and many more. The COVID-19 pandemic imposes a positive indication of the recovery of environmental degradation through improving the physical environmental parameters [1]. Restriction on human movement, industrial production, and vehicle movement results in the reduction of PM_{10} concentration in the atmosphere; on the other hand, less anthropogenic heat flux in the near-surface atmosphere resulting from human movement has also reduced LST, which helps to minimize the natural increase of LST from its previous year [54]. Not only these two parameters, but some biophysical parameters such as NDVI, NDWI, and NDMI have also changed due to uninterrupted or untouched condition of the natural environment.

The result indicates that overall environmental quality of all the study sites has improved during lockdown time, although the better environmental quality is found during the pre-lockdown time, which is the combination of two factors: (1) imposition of restriction rules in megacities of India before declaring formal lockdown for the whole country, (2) seasonal variation due to changes in data collection months. Most of the satellite images for pre-lockdown time were collected from February and the first half of March, which is the transition time between winter and summer season, but lockdown satellite images were collected mostly from April, except for Kolkata, which was collected for 29 March, which represents hotter days than pre-lockdown time.

National Capital Region (NCR) Delhi has repeatedly come into headlines of a reputed Indian newspaper for degraded air quality during the last 3 to 4 months [2], and other studied megacities are also in the same direction of degraded air quality, but COVID-19 lockdown on these megacities has shown a drastic change in the air quality, especially in PM_{10} concentration. LST has also been showing a similar increasing trend for the last few years, which is also reduced in this time for a lesser amount of

vehicle and human exposure to the environment. Inter-megacity comparison of environmental quality indicates that Chennai has better environmental quality than the other three megacities under this study because of its locational advantage of being a coastal city, which generally reduces the amount of LST for the whole year compared to landlocked megacities.

In NCR, Delhi PM₁₀ concentration was less in pre-lockdown time. It could be due to several reasons such as: (i) imposition of different regulation, i.e., allowing odd- and even-number vehicles on the road on alternative days, (ii) continuous water spray on roads for reducing the supply of particulate matters, etc., for minimizing air pollution through reducing particulate matter concentration in the air. These regulations play a positive role in minimizing air pollution and overall environmental quality of the studied cities. In the case of Kolkata, the less temperate condition may play an important role in minimizing PM₁₀ concentration in the air.

Overall, this study found that the environmental quality of the studied megacities has improved from its previous years; in some instances, it is also improved from pre-lockdown time. This positive indication is generating some hope for people to get a better and recovered environmental condition, irrespective of this deadliest pandemic situation.

7. Conclusions

Changing environmental quality of the world has gained a positive move toward sustainable environment-friendly conditions due to the imposition of the lockdown owing to the COVID-19 pandemic. Environmental parameters such as PM₁₀ concentration, NDWI, and NDMI have changed positively during this lockdown time, which is already assessed by some conducted and published studies. To the best of our knowledge, this is the first study that tries to present the changes in the environmental conditions due to the imposition of lockdown comprehensively owing to COVID-19 by devising an environmental quality index. The study found that overall environmental quality has improved from its previous year (same months) for all four studied megacities, although according to the general trend of environmental quality degradation, 2020 must have the worst environmental condition than the environmental condition of 2019. The environmental quality index map indicates an improved environmental condition, which is a sign of anticipation for the environmentalist in this crisis moment. This study has tried to obtain an overall view of the environmental condition, but more detailed investigation is still needed for a better understanding of the environmental response to the COVID-19 pandemic imposed lockdown situation and assessment of UQI after the lockdown situation is also important for understanding the environmental impact of COVID-19 specifically. However, the lockdown situation is still existing in India; hence, after the lockdown, a more detailed investigation on these aspects will help to maintain the better quality of environment.

Author Contributions: Methodology; formal analysis, S.G., A.D., T.K.H., and S.S.; S.G. and S.S., investigation; writing—original draft preparation, S.G., A.D., and T.K.H., S.S.; writing—review and editing, B.P. and S.S., and S.G. performed the experiments, wrote the manuscript; S.S. wrote the manuscript and analyzed the data; B.P. supervised, edited, restructured, and professionally optimized the manuscript; B.P. and A.M.A. arranged the funding acquisition. All authors have read and agreed to the published version of the manuscript.

Funding: This research is supported by the Centre for Advanced Modelling and Geospatial Information Systems (CAMGIS), Faculty of Engineering and IT, the University of Technology Sydney (UTS). This research was also supported by Researchers Supporting Project number RSP-2020/14, King Saud University, Riyadh, Saudi Arabia.

Conflicts of Interest: The authors declare no conflict of interest.

References

1. Mahato, S.; Pal, S.; Ghosh, K.G. Effect of lockdown amid COVID-19 pandemic on air quality of the megacity Delhi, India. *Sci. Total Environ.* **2020**, *730*, 139086. [[CrossRef](#)] [[PubMed](#)]
2. Sharma, S.; Mathur, S. Analyzing the Patterns of Delhi's Air Pollution. In *Advances in Data Sciences, Security and Applications*; Springer: Singapore, 2020; pp. 33–44.

3. Mukherjee, A.; Agrawal, M. Air pollutant levels are 12 times higher than guidelines in Varanasi, India. Sources and transfer. *Environ. Chem. Lett.* **2018**, *16*, 1009–1016. [[CrossRef](#)]
4. Garaga, R.; Sahu, S.K.; Kota, S.H. A review of air quality modeling studies in India: Local and regional scale. *Curr. Pollut. Rep.* **2018**, *4*, 59–73. [[CrossRef](#)]
5. Guo, H.; Kota, S.H.; Sahu, S.K.; Hu, J.; Ying, Q.; Gao, A.; Zhang, H. Source apportionment of PM_{2.5} in North India using source-oriented air quality models. *Environ. Pollut.* **2017**, *231*, 426–436. [[CrossRef](#)] [[PubMed](#)]
6. World Health Organization. Ambient Air Pollution: A Global Assessment of Exposure and Burden of Disease. 2016. Available online: <http://who.int/phe/publications/airpollution-globalassessment/en/> (accessed on 20 May 2020).
7. Polk, H.S. *State of Global Air 2019: A Special Report on Global Exposure to Air Pollution and Its Disease Burden*; Health Effects Institute: Boston, MA, USA, 2019.
8. Mohan, M.; Kandya, A. Impact of urbanization and land-use/land-cover change on diurnal temperature range: A case study of tropical urban airshed of India using remote sensing data. *Sci. Total Environ.* **2015**, *506*, 453–465. [[CrossRef](#)] [[PubMed](#)]
9. Haque, M.; Singh, R.B. Air pollution and human health in Kolkata, India: A case study. *Climate* **2017**, *5*, 77. [[CrossRef](#)]
10. Sharma, R.; Chakraborty, A.; Joshi, K. Geospatial quantification and analysis of environmental changes in urbanizing city of Kolkata (India). *Environ. Monit. Assess.* **2015**, *187*, 4206. [[CrossRef](#)]
11. Kumar, A.; Gupta, I.; Brandt, J.; Kumar, R.; Dikshit, A.K.; Patil, R.S. Air quality mapping using GIS and economic evaluation of health impact for Mumbai city, India. *J. Air Waste Manag. Assoc.* **2016**, *66*, 470–481. [[CrossRef](#)]
12. Sundaram, A.M. Urban green-cover and the environmental performance of Chennai city. *Environ. Dev. Sustain.* **2011**, *13*, 107–119. [[CrossRef](#)]
13. Partheeban, P.; Raju, H.P.; Hemamalini, R.R.; Shanthini, B. Real-Time Vehicular Air Quality Monitoring Using Sensing Technology for Chennai. In *Transportation Research*; Springer: Singapore, 2020; pp. 19–28.
14. Sathyakumar, V.; Ramsankaran, R.; Bardhan, R. Geospatial approach for assessing spatiotemporal dynamics of urban green space distribution among neighbourhoods: A demonstration in Mumbai. *Urban For. Urban Green.* **2020**, *48*, 126585. [[CrossRef](#)]
15. Liang, B.; Weng, Q. Assessing urban environmental quality change of Indianapolis, United States, by the remote sensing and GIS integration. *IEEE J. Sel. Top. Appl. Earth Obs. Remote Sens.* **2010**, *4*, 43–55. [[CrossRef](#)]
16. Akbari, H.; Rosenfeld, A.H.; Taha, H. Summer heat islands, urban trees, and white surfaces. *ASHRAE Trans.* **1990**, *96*, 1381–1388.
17. Akbari, S.; Rose, H.L.S.; Taha, H. Analyzing the land cover of an urban environment using high-resolution orthophotos. *Landsc. Urban Plan.* **2003**, *63*, 1–14. [[CrossRef](#)]
18. De Vries, S.; Verheij, R.A.; Groenewegen, P.P.; Spreeuwenberg, P. Spreeuwenberg, Natural environments—Healthy environments? An exploratory analysis of relationship between green space and Health. *Environ. Plan. A* **2003**, *35*, 1717–1731. [[CrossRef](#)]
19. Nichol, J.; Wong, M.S. Modeling urban environmental quality in a tropical city. *Landsc. Urban Plan.* **2005**, *73*, 49–58. [[CrossRef](#)]
20. Heynen, N. Green urban political ecologies: Toward a better understanding of inner-city environmental change. *Environ. Plan A* **2006**, *38*, 499–516. [[CrossRef](#)]
21. Weng, Q.; Lu, D.; Schubring, J. Estimation of land surface temperature–vegetation abundance relationship for urban heat island studies. *Remote Sens. Environ.* **2004**, *89*, 467–483. [[CrossRef](#)]
22. Weng, Q.; Liu, H.; Liang, B.; Lu, D. The spatial variations of urban land surface temperatures: Pertinent factors, zoning effect, and seasonal variability. *IEEE J. Sel. Top. Appl. Earth Obs. Remote Sens.* **2008**, *1*, 154–166. [[CrossRef](#)]
23. Rajasekar, U.; Weng, Q. Spatio-temporal modelling and analysis of urban heat islands by using Landsat TM and ETM+ imagery. *Int. J. Remote Sens.* **2009**, *30*, 3531–3548. [[CrossRef](#)]
24. Li, G.; Weng, Q. 15 Integration of Remote Sensing and Census Data for Assessing Urban Quality of Life: Model Development. In *Urban Remote Sensing*; Weng, Q., Quattrochi, D.A., Eds.; CRC Press: Boca Raton, FL, USA, 2006; p. 311.
25. Li, G.; Weng, Q. Measuring the quality of life in city of Indianapolis by integration of remote sensing and census data. *Int. J. Remote Sens.* **2007**, *28*, 249–267. [[CrossRef](#)]

26. Zhang, X.; Wang, C.; Li, E.; Xu, C. Assessment model of ecoenvironmental vulnerability based on improved entropy weight method. *Sci. World J.* **2014**, *2014*, 797814. [CrossRef]
27. Sharma, S.; Zhang, M.; Gao, J.; Zhang, H.; Kota, S.H. Effect of restricted emissions during COVID-19 on air quality in India. *Sci. Total Environ.* **2020**, *728*, 138878. [CrossRef]
28. Mohan, M.; Dagar, L.; Gurjar, B.R. Preparation and validation of gridded emission inventory of criteria air pollutants and identification of emission hotspots for megacity Delhi. *Environ. Monit. Assess.* **2007**, *130*, 323–339. [CrossRef] [PubMed]
29. Saraswat, I.; Mishra, R.K.; Kumar, A. Estimation of PM10 concentration from Landsat 8 OLI satellite imagery over Delhi, India. *Remote Sens. Appl. Soc. Environ.* **2017**, *8*, 251–257. [CrossRef]
30. Landsat Missions: Using the USGS Landsat 8 Product. Available online: <https://landsat.usgs.gov/using-usgs-landsat-8-product> (accessed on 15 December 2016).
31. Landsat Project Science Office. *Landsat 7 Science Data User's Handbook*; Goddard Space Flight Center, NASA, 2002. Available online: http://ftpwww.gsfc.nasa.gov/IAS/handbook/handbook_toc.html (accessed on 20 May 2020).
32. Nichol, J.E. A GIS-based approach to microclimate monitoring in Singapore's high-rise housing estates. *Photogramm. Eng. Remote Sens.* **1994**, *60*, 1225–1232.
33. Artis, D.A.; Carnahan, W.H. Survey of emissivity variability in thermography of urban areas. *Remote Sens. Environ.* **1982**, *12*, 313–329. [CrossRef]
34. Snyder, W.C.; Wan, Z.; Zhang, Y.; Feng, Y.Z. Classification-based emissivity for land surface temperature measurement from space. *Int. J. Remote Sens.* **1998**, *19*, 2753–2774. [CrossRef]
35. Chen, X.L.; Zhao, H.M.; Li, X.; Yin, Z.Y. Remote sensing image-based analysis of the relationship between urban heat island and land use/cover changes. *Remote Sens. Environ.* **2006**, *104*, 133–146. [CrossRef]
36. Jackson, T.J.; Chen, D.; Cosh, M.; Li, F.; Anderson, M.; Walthall, C.; Doriaswamy, P.; Hunt, E.R. Vegetation water content mapping using Landsat data derived normalized difference water index for corn and soybeans. *Remote Sens. Environ.* **2004**, *92*, 475–482. [CrossRef]
37. Gao, B.C. NDWI—A normalized difference water index for remote sensing of vegetation liquid water from space. *Remote Sens. Environ.* **1996**, *58*, 257–266. [CrossRef]
38. Purevdorj, T.S.; Tateishi, R.; Ishiyama, T.; Honda, Y. Relationships between percent vegetation cover and vegetation indices. *Int. J. Remote Sens.* **1998**, *19*, 3519–3535. [CrossRef]
39. Nguyen, A.K.; Liou, Y.A.; Li, M.H.; Tran, T.A. Zoning eco-environmental vulnerability for environmental management and protection. *Ecol. Indic.* **2016**, *69*, 100–117. [CrossRef]
40. Jin, S.; Sader, S.A. Comparison of time series tasseled cap wetness and the normalized difference moisture index in detecting forest disturbances. *Remote Sens. Environ.* **2005**, *94*, 364–372. [CrossRef]
41. Ghosh, S.; Das, A. Urban expansion induced vulnerability assessment of East Kolkata Wetland using Fuzzy MCDM method. *Remote Sens. Appl. Soc. Environ.* **2019**, *13*, 191–203. [CrossRef]
42. Keshavarzi, A.; Sarmadian, F.; Heidari, A.; Omid, M. Land suitability evaluation using fuzzy continuous classification (a case study: Ziaran region). *Mod. Appl. Sci.* **2010**, *4*, 72. [CrossRef]
43. Hembram, T.K.; Saha, S. Prioritization of sub-watersheds for soil erosion based on morphometric attributes using fuzzy AHP and compound factor in Jainti River basin, Jharkhand, Eastern India. *Environ. Dev. Sustain.* **2018**, *6*, 1–28. [CrossRef]
44. Ahmed, R.; Sajjad, H.; Husain, I. Morphometric parameters-based prioritization of sub-watersheds using fuzzy analytical hierarchy process: A case study of lower Barpani Watershed, India. *Nat. Resour. Res.* **2017**, *27*, 67–75. [CrossRef]
45. Mamdani, E.H. Application of fuzzy logic to approximate reasoning using linguistic synthesis. *IEEE Trans. Comput.* **1977**, *12*, 1182–1191. [CrossRef]
46. Bojadziev, G. *Fuzzy Logic for Business, Finance, and Management*; World Scientific: Singapore, 2007; Volume 23.
47. Sarkar, S.; Parihar, S.M.; Dutta, A. Fuzzy risk assessment modelling of East Kolkata Wetland Area: A remote sensing and GIS based approach. *Environ. Model. Softw.* **2016**, *75*, 105–118. [CrossRef]
48. Saaty, T.L. A scaling method for priorities in hierarchical structures. *J. Math. Psychol.* **1977**, *15*, 234–281. [CrossRef]
49. Saaty, T.L. *The Analytical Hierarchy Process*; McGraw Hill: New York, NY, USA, 1980; p. 350.
50. Saha, S. Groundwater potential mapping using analytical hierarchical process: A study on Md. Bazar Block of Birbhum District, West Bengal. *Spat. Inf. Res.* **2017**, *25*, 615–626. [CrossRef]

51. Satty, T.L.; Vargas, L.G. Models, methods, concepts and applications of the analytic hierarchy process. *Int. Ser. Oper. Res. Manag. Sci.* **2001**, *34*, 1–352.
52. Mondal, B.; Dolui, G.; Pramanik, M.; Maity, S.; Biswas, S.S.; Pal, R. Urban expansion and wetland shrinkage estimation using a GIS-based model in the East Kolkata Wetland, India. *Ecol. Indic.* **2017**, *83*, 62–73. [[CrossRef](#)]
53. Richardson, C.; Amankwatia, K. GIS-based analytic hierarchy process approach to watershed vulnerability in Bernalillo County, New Mexico. *J. Hydrol. Eng.* **2018**, *23*, 04018010. [[CrossRef](#)]
54. Muhammad, S.; Long, X.; Salman, M. COVID-19 pandemic and environmental pollution: A blessing in disguise? *Sci. Total Environ.* **2020**, *20*, 138820. [[CrossRef](#)]



© 2020 by the authors. Licensee MDPI, Basel, Switzerland. This article is an open access article distributed under the terms and conditions of the Creative Commons Attribution (CC BY) license (<http://creativecommons.org/licenses/by/4.0/>).